ISSN 1069-3513, Izvestiya, Physics of the Solid Earth, 2014, Vol. 50, No. 4, pp. 576–587. © Pleiades Publishing, Ltd., 2014.
Original Russian Text © V.O. Mikhailov, E.A. Kiseleva, E.I. Smol'yaninova, P.N. Dmitriev, V.I. Golubev, Yu.S. Isaev, K.A. Dorokhin, E.P. Timoshkina, S.A. Khairetdinov, 2014, published in Fizika Zemli, 2014, No. 4, pp. 120–130.

Some Problems of Landslide Monitoring Using Satellite Radar Imagery with Different Wavelengths: Case Study of Two Landslides in the Region of Greater Sochi

V. O. Mikhailov[a], E. A. Kiseleva[a], E. I. Smol'yaninova[a], P. N. Dmitriev[a], V. I. Golubev[a], Yu. S. Isaev[b], K. A. Dorokhin[b], E. P. Timoshkina[a], and S. A. Khairetdinov[a]

[a] *Schmidt Institute of Physics of the Earth, Russian Academy of Sciences, ul. Bol'shaya Gruzinskaya 10, Moscow, 123995 Russia*
e-mail: mikh@ifz.ru

[b] *OAO Lenmetrogiprotrans Scientific Research and Design Institute, ul. Bol'shaya Moskovskaya 2, St. Petersburg, 191002 Russia*

Received February 19, 2014

Abstract—The problems of processing and interpreting the data provided by radar satellite interferometry for the conditions of landslides covered by vegetation are analyzed in two case studies of landslides in the Northern Caucasus in the region of Kepsha and Mamaika villages in the vicinity of the railway tunnels. The estimates of the displacement fields are obtained by the method of persistent scatterers using the StaMPS program package. The five-year experience of landslide monitoring shows that in the unfavorable conditions of satellite radar interferometry, proper selection of the strategy of satellite image processing is vital. In the present paper, we discuss, in particular, the crop selection, the selection of the master image, reference area, and digital elevation model. For the landslide located in the sparsely populated region near Kepsha village, we used the data from the ascending and descending tracks of the long-wavelength ALOS and shorter-wavelength ENVISAT satellites. For the landslide in the region of Mamaika village with a large number of different buildings serving as good scatterers for radar signals, we used the images from the ENVISAT and from TerraSAR satellite, which transmits even shorter waves. The average line-of-sight (LOS) displacement velocities V_{LOS} for the landslide near Kepsha village measure at most 10 mm per annum, which means that this landslide has remained stable at least since 2004. The landslide in Mamaika village is significantly more active. The average LOS displacement velocities in the active part of this landslide attain 60 mm per annum. The artificial corner reflector installed on the segment of the landslide where natural scatterers of radar signal are absent made it possible to estimate the LOS displacement velocity on this segment of the slope at 49 mm per annum.

DOI: 10.1134/S1069351314040107

1. INTRODUCTION

Satellite radar interferometry is nowadays one of the actively developing directions in the Earth's studies from space. The images taken by the interferometric synthetic aperture radars (InSAR) are used for constructing digital elevation models (DEM) and estimating subtle displacements of the Earth's surface and engineering objects. The first estimates of the surface displacements were obtained with the use of interferograms generated based on two radar images obtained from locally parallel orbits (the so called differential interferomety, DInSAR). The interferograms show the relative phase shift of two reflected radar signals measured during the repeated surveying of the same object. This phase shift is due to the displacement of the reflecting object during the time interval between the surveys; however, it also depends on the changes in the atmospheric conditions, vegetation, and snow cover. The errors of orbit determination and DEM also contributed to the phase shift. This significantly reduces the possibilities of the methods of differential interferometry, although there are extensive publications on determining the displacement fields in the regions of the earthquakes, exploitation of oil and gas deposits, on the glaciers, and volcanoes by DInSAR methods. The review of some results can be found, for instance, in (Mikhailov et al., 2010; 2012).

Various methods for solving the problems of differential interferometry have been developed so far. One of the suggested approaches is the persistent scatterer (PS) techniques. The main idea of these methods (referred to as the PS-InSAR techniques) is to simultaneously analyze a series of interferograms, on which only the pixels with a stable, in a certain sense, behavior are identified and used in the further study (Ferretti et al., 2001). The existing algorithms of PS-InSAR methods differ, inter alia, by the mathematical formalism of stable behavior. For example, in the methods suggested in (Ferretti et al., 2000; Crosetto et al., 2003; Colesanti et al., 2003; Lyons and Sandwell, 2003; Adam et al., 2009), the initial set of PSs is composed of the pixels corresponding to the scattered signal with

a high amplitude. Many approaches postulate the time dependence of PS displacements, assuming it to be linear, periodic, etc. These methods are efficient in the urban and industrial terrains where there are many objects with a high and stable amplitude of the scattered radar signal. Alongside this, the number of PSs identified in the areas where the buildings and constructions are absent is small. Nevertheless, there are many examples of efficient application of these algorithms to the natural objects including landslides (e.g., Kimura and Yamaguchi, 2000; Colesanti and Wasowski, 2006; Farina et al., 2006; Farina et al., 2007; Meisina et al., 2007; Brugioni et al., 2011).

A series of methods were suggested for identifying the PSs in the natural objects, where the scattered signals have far lower amplitudes. One of these approaches is based on the assumption that the displacement field of the natural objects is in some way correlated in space and time. Due to this, it is possible to distinguish the surface deformation signal against the noise, which is high-frequency in space (instrumental noise) and time (atmospheric effects and errors in satellite tracking). Among these approaches, we point out the method suggested by A. Hooper (Hooper et al., 2004) and implemented in the StaMPS (Stanford Methods for Persistent Scatterers) program package and the SqueeSAR method (Ferretti et al., 2011).

In the present study, we consider some of the main problems associated with applying the PS method for estimating the displacement fields of natural objects by the example of two landslide slopes in the region of Greater Sochi in the Northern Caucasus. We analyze the radar images from the ascending and descending tracks of the ALOS and ENVISAT satellites, as well as the images from the TerraSAR satellite acquired at a different time. At the beginning of the paper, we outline the general characteristic of the regions of study—the landslides in the vicinity of Kepsha village and in Mamaika village—and review the satellite data used for the analysis. Then, we briefly describe the method used for satellite image processing, discuss the general strategy of processing, and examine some approaches specially designed for the study. The results of the calculations, the interpretation, and discussion conclude the paper.

2. THE REGIONS OF STUDY AND SATELLITE DATA

We have studied two landslides at the foothills of the Greater Caucasus. One landslide is located near Kepsha village in the vicinity of the tunnel of the newly constructed road connecting Adler and Krasnaya Polyana, and another, in the northern suburb of Sochi in Mamaika village above the tunnel of the Tuapse–Sochi railroad. The landslide bodies are composed of marlstone interbedded by clays, which lose their strength when saturated with water.

The conditions for applying SAR interferometry in these two regions are strikingly different. The Mamaika landslide is located within the territory of urban development of Sochi, where there are scores of engineering objects that reflect the satellite radar signals quite well. The landslide in the region of Kepsha village is a slope that is almost fully covered by vegetation, where the scattering conditions are much worse. In both cases, we had no data of the ground instrumental observations; therefore, it was only possible to verify the results of satellite image processing by visual observations.

The landslide slope in the region of Kepsha village has a size of 500 × 800 m and a steeper upper part. The height contrast is 200 to 1200 m. The landslide slope is strongly water-saturated and almost fully covered by various species of subtropical vegetation. All this, together with the sparse coverage of this area by the well-scattering constructions impede the application of SAR interferometry.

For studying the landslide near Kepsha village, we used the SAR images taken by the ENVISAT satellite (*C*-band with a wavelength of 5.6 cm) covering the interval from August 2004 to March 2012 and the images from the Japanese ALOS satellite (*L*-band signals with a wavelength of 23.4 cm) for the period from January 2007 to September 2010. The time intervals of the surveys and the distances between the survey points (baselines) are shown in Fig. 1a. The survey geometry is illustrated in the corresponding figures displaying the results of the calculations.

The interval of surveying from the ascending track 85A of the ENVISAT satellite partially overlaps the surveying interval from the ascending orbital track 588A of the ALOS satellite. Since ENVISAT was placed in a new orbit in October 2010, the joint processing of the entire series of images from the descending 35D orbital track is impossible. We have grouped the images from this track into two series, one for the interval before orbit correction (November 2007 to July 2010) and the other, after the correction (November 2010 to March 2012). These series include 12 and 13 satellite images, respectively.

In terms of the size, the Mamaika landslide does not significantly differ from the landslide in Kepsha village: its landslide slope is about 600 × 800 m. However, here, the topography is quite smooth, and the difference in the heights is rather small (0 to 300 m). The landslide is located in a densely populated region with many buildings and constructions, which are perfect scatterers for the satellite radar signals. This provides quite favorable conditions for radar interferometry.

The images from ENVISAT tracks 85A and 35D (Fig. 1a) also cover the region of the Mamaika landslide. Since 2011, we have started requesting the images from TerraSAR satellite (track 54A), which span the interval from December 24, 2011 to May 24, 2013 (Fig. 1b). The southern margin of the landslide immediately above the tunnel is void of the scattering targets; therefore, we installed the artificial corner reflector (CR) on November 22, 2012 there. CR with a side of 1 m is made of black metal and is aluminum paint to protect it from corrosion (Fig. 2).

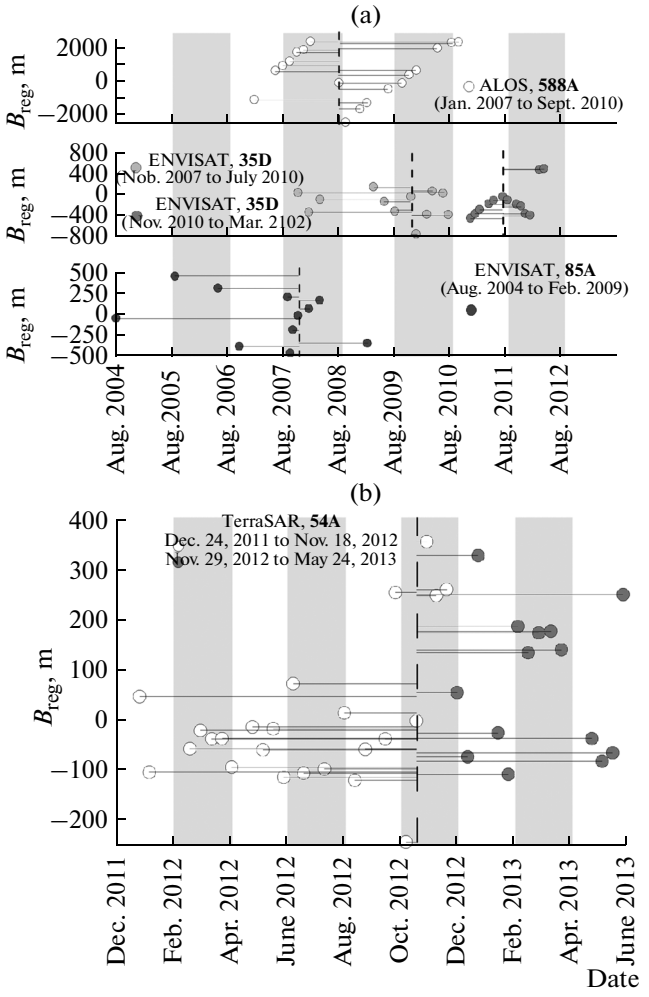

Fig. 1. The radar images used for studying the landslide processes: (a) in the region of Kepsha village; (b) in the region of Mamaika village.

3. THE PROCEDURE OF SAR IMAGE PROCESSING

The method suggested by A. Hooper and implemented in the StaMPS program package (Hooper et al., 2004) is intended for identifying PSs in poorly reflecting natural terrains. This method analyzes the phase stability of the reflected signal over time assuming that the displacement field is temporally and spatially correlated. It is remarkable that this method does not hypothesize the time dependence of the displacement velocity. This is particularly important for the natural objects whose displacement velocity can significantly vary with time, and fixing the intervals of activation of these displacements is one of the problems addressed by SAR interferometry.

Identifying the PS and constructing the time series of the displacements is implemented in three steps. At the first step, the phase stability of each pixel is estimated. The second step is direct selection of the persistent scatterers from the entire set of pixels. At the third step, phase unwrapping is conducted, and deformation is estimated for the selected stable targets. The StaMPS package also includes the algorithms for mitigating the atmospheric effects and reducing the DEM-related errors, as well as the algorithms for the three-dimensional phase unwrapping in time and space (Hooper et al.,, 2007).

Fig. 2. The corner reflector installed in the lower part of the landslide slope near Mamaika village.

The difficulty in selecting stable scattering targets for estimating the displacement field is associated with the fact that the phase from each element of the interferogram is the sum of five phase components wrapped modulo 2π:

$$\varphi_{i,j} = W\left[\varphi_{def,i,j} + \varphi_{\alpha,i,j} + \varphi_{orb,i,j} + \varphi_{\theta,i,j} + n_{i,j}\right], \qquad (1)$$

where $\varphi_{def,i,j}$ is the phase contribution due to the displacement of the reflecting target towards the satellite; $\varphi_{\alpha,i,j}$ is the phase associated with the change in the conditions of atmospheric propagation of electromagnetic waves between two acquisitions; $\varphi_{orb,i,j}$ is the phase shift caused by orbit errors; $\varphi_{\theta,i,j}$ is the phase contribution due to the errors in the determination of the look angle of the satellite; $n_{i,j}$ is the contribution of various noise (including instrumental) and unaccounted errors; and W is the operator of modulo 2π wrapping. Here, index i denotes the number of the interferogram, and j denotes the pixel number in it. By definition, the pixel is assumed to be stably reflecting if the noise from this pixel is low compared to the other components.

Component $\varphi_{\theta,i,j}$ is directly proportional to the perpendicular baseline $B_\perp$, which is the distance along the normal dropped from the point of acquisition of the repeated pass towards the ray direction from the acquisition point of the first pass. Since $B_\perp$ is known quite accurately, this component is efficiently removed (Hooper et al., 2004). Let us now compare the character of variations in the other phase components in

Eq. (1) in space and time. Many natural phenomena (landslides, glaciers, volcanoes, displacements on the tectonic faults) and some anthropogenic processes have been evolving irregularly in time: periods of drastic activation alternate with periods of slow motion. The PS methods are applied just for fixing the slow motion. Here, it is important that for many slowly evolving natural processes it can be hypothesized that the displacement field is temporally and spatially correlated. The characteristic scale of variations in the atmospheric conditions is typically larger than a few km; therefore, the atmospheric delays of the signals are spatially correlated within a single image but noticeably different over a series of successive images; i.e., they are temporally decorrelated. The orbital errors also produce phases that slowly vary in space but are not correlated between the successive images. Based on these relationships, we can separate the first four long-period components in the right-hand side of Eq. (1) after bandpass filtering of the interferograms over the spatial coordinates and eliminating the phase component proportional to $B_\perp$. Thus, we obtain an estimate of the noise $n_{i,j}$ that is neither spatially nor temporally correlated (Hooper et al., 2004). From the noise estimate, we can calculate the phase dispersion for each pixel and select those pixels from which the noise dispersion does not exceed a given threshold.

The processing of the SAR image and identifying the PSs include a series of procedures. In particular, it is required to optimally crop the studied area in the images, to specify the parameters of bandpass filtering, to reject the images with high noise level; and to specify the area relative to which the displacements will be calculated (the reference area). In complicated conditions, when there are only few radar images and they are weakly coherent, the results can strongly depend on the selected processing strategy. General hints on performing particular steps of the processing can be found in (Hooper et al., 2010). Below we describe some special approaches that we applied at certain stages of processing, taking into account the specificity of the studied regions.

Selecting the Image Crop

The radar images cover huge territories; therefore, it is common practice to crop an area of interest in the image for further study in order to reduce the time of computations. In contrast to the regions with a smooth topography, the crop area in mountainous regions should be selected with particular thoroughness. When changing the size of the area of computations, one should include or exclude the mountain peaks or valleys with rugged topography and varying atmospheric conditions, as well as the steep slopes characterized by large DEM offsets. The optimal size of the area of study in mountainous terrains should be rather small to minimize the height differences within it; however, the area should be sufficiently large to avoid the boundary effects and provide efficient image matching (the so-called coregistration).

Taking into account these factors and the pixel size in the images from different satellites, for the landslide near Kepsha village, we selected box-shaped crop with a size of 3500 pixels along the satellite path and 700 pixels perpendicular to it for ENVISAT images; the crop for ALOS images was 4700 × 800 pixels. The calculations for the crops having similar sizes show that the estimates of the displacement fields are robust. The size of the crop for the Mamaika landslide does not affect the results of the calculations since the topography is gentle and the height contrast is rather low.

Selecting the Master Image

In the technology of persistent scatterers, all the images should be coregistered with a certain image, which is referred to as the master. The master image should be best correlated with all the images of a given series. For selecting the master image, we initially picked a few images with small baseline components (perpendicular $B_\perp$ and time T) and Doppler frequency F_{DC} based on the functional (Hooper et al., 2007):

$$\rho_{\text{total}} = \rho_{\text{temporal}}\rho_{\text{spatial}}\rho_{\text{doppler}}\rho_{\text{thermal}}$$
$$\approx \left(1 - f\left(\frac{T}{T^c}\right)\right)\left(1 - f\left(\frac{B_\perp}{B_\perp^c}\right)\right)\left(1 - f\left(\frac{F_{DC}}{F_{DC}^c}\right)\right)\rho_{\text{thermal}}, \quad (2)$$

where $f(x) = \begin{cases} x, & x \le 1 \\ 1, & x > 1 \end{cases}$, T^c, $B_\perp^c$, and F_{DC}^c are the critical values of the corresponding parameters at which the coefficient of correlation is zero. The value of ρ_{thermal}, which characterizes the instrumental noise, was assumed to be constant.

For each candidate for a master image, we calculated the interferogram pairs with all the images of the series and constructed the corresponding coherence maps by the following formula:

$$\gamma_j = \frac{\left|E(z_1 z_2^*)\right|}{\sqrt{E(z_1 z_1^*)E(z_2 z_2^*)}}, \quad (3)$$

where $E(\ )$ is the operator of averaging over a spatial ensemble, z_1 and z_2 are the complex-valued signals corresponding to the same scene (the areas on the surface of the Earth) in the two images forming the differential interferogram, and * is the operator of complex conjugate. The coherence map is a matrix in which each element is equal to the value of the coherence corresponding to its scene element on the Earth's surface (the pixel of the differential interferogram). The interferometric coherence is a real-valued quantity ranging from 0 to 1; it reflects the degree of decorrelation between two images. Decorrelation is contributed by a number of sources, including a low signal-to-noise ratio, atmospheric noise, snow, and long time gap between the acquisitions. In our analysis, the image for which the interferograms have the best

coherence with all the other images of a series in the studied area has been eventually selected as the master image. This approach not only considers the geometry of the survey but also takes into account the contributions of the atmosphere, vegetation, and snow cover.

It is worth noting that the suggested procedure for selecting the master image should be applied for a particular studied area since the coherence is not identical in different segments of the image: the coherence in the densely populated regions is barely sensitive to the vegetation cycles, whereas in the forested areas it is significantly season-dependent. The landslides in the region of Kepsha village are covered with snow for a few months in winter. In the region of Mamaika, snow cover only persists for a few days. Thus, the master image selected for the calculations over different segments of the image is not necessarily the same.

Digital Elevation Model (DEM)

DEM is required to eliminate the topographic phases. In our study, we have analyzed three DEMs: SRTM3, ACE-2, and ASTER. For the landslide near Kepsha village, the heights at the characteristic points of the three models were compared to the corresponding values read from the detailed surface topography map. The height differences in the eastern part of the landslide, which is ravined by streams, attain 30 m. The ACE-2 and SRTM3 models provide an identical degree of detail (90 m); however, SRTM3 has the gaps in the west segment of the studied area in the region of the Mzymta river valley, which can result in errors. The degree of detail of ASTER DEM is much higher (30 m); at the same time, in the central part of the Kepsha landslide the heights differ by 8 m from the corresponding values in the SRTM3 and ACE-2 models and from the ground geodetic data. The ASTER model is based on the optical data, and in the conditions of densely vegetated terrain, it corresponds to the tops of the trees. The landslide near Kepsha village is almost completely covered by various vegetation ranging from dense shrublets to lofty relic trees; therefore, in this case we selected the ACE2 DEM, which is coarser but better fits the ground data. For the Mamaika landslide, where the vegetation cover is far less extensive, we used the finer-detail ASTER model.

Selecting the Reference Area

SAR interferometry is only capable of estimating the relative displacements; therefore, a reference point or reference area should be specified in order to fix these displacements. By default, the displacements in the StaMPS package are calculated with respect to the average phase over the entire studied area. This is acceptable when processing large images, where spatial averaging suppresses the different noise and the overall motion of the area can be assumed to be zero. If a significant part of the area is occupied by the landslide, the average displacement could probably be nonzero. In this case, the estimates of the landslide velocity will be undervalued, while the stable segments will apparently start moving in the opposite direction to the landslide. When selecting the reference area, we set two criteria: (1) the reference area should be stable during the survey interval; (2) this area should be located as close as possible to the landslide so that the atmospheric and other artifacts within the landslide and within the stable area are similar. Since the region of Kepsha village hosted extensive building activities, it was impossible to specify a known stable area there; therefore, the reference area was selected in accordance with the coherence estimates.

This was done by the following procedure. First, based on the calculated coherence maps, we localized the highly coherent pixels assuming that they are most likely to correspond to the manmade scatterers. These targets are simpler to identify in the images and they are more likely to turn out to be stable. Due to the specificity of the procedure of selecting the stable scatterers applied in the StaMPS package, not all the highly coherent pixels are picked out as the PSs and, correspondingly, could be considered as a reference area. Therefore, at the first step, we selected a few (N) small, highly coherent areas that included at most three PSs. Then, we calculated the time series of the displacements $W_{ij}(t)$ for all the candidate areas ($i = 1,2,..., N$) by successively selecting each area ($j = 1,2,..., N, i \neq j$) as the reference area. If for two areas k and l that are sufficiently distant from each other, the time series of the displacements $W_{kl}(t)$ did not contain a noticeable time trend and if the variance of the time series was rather low, both areas were considered stable and suitable for use as the reference areas. As a result of applying this procedure, at least two possible reference areas are selected. When conducting the calculations for the landslide slope, it is reasonable to select the reference area that is closest to the landslide. In this case, the time series for the reference area and the time series for the landslide will most probably contain the same noise, which is eliminated in the calculations with the selected reference area.

As mentioned above, in the conditions of sparse targets that reflect the radar signals quite well and with the rather short time series of the images, the results may turn out to be dependent on the strategy of processing and on the selected parameters. In our study, we conducted extensive calculations with different values of the parameters and different master images. The results in which the number of the identified stable reflecting targets was maximal provided that the root mean square (rms) deviation of their displacement velocities from the linear trend did not exceed the given limit were treated as the best.

4. THE RESULTS OF THE CALCULATIONS AND DISCUSSION

Figures 3–6 show the results of calculating the average displacement velocities projected on LOS (V_{LOS}) for the stably persistent scatterers identified on

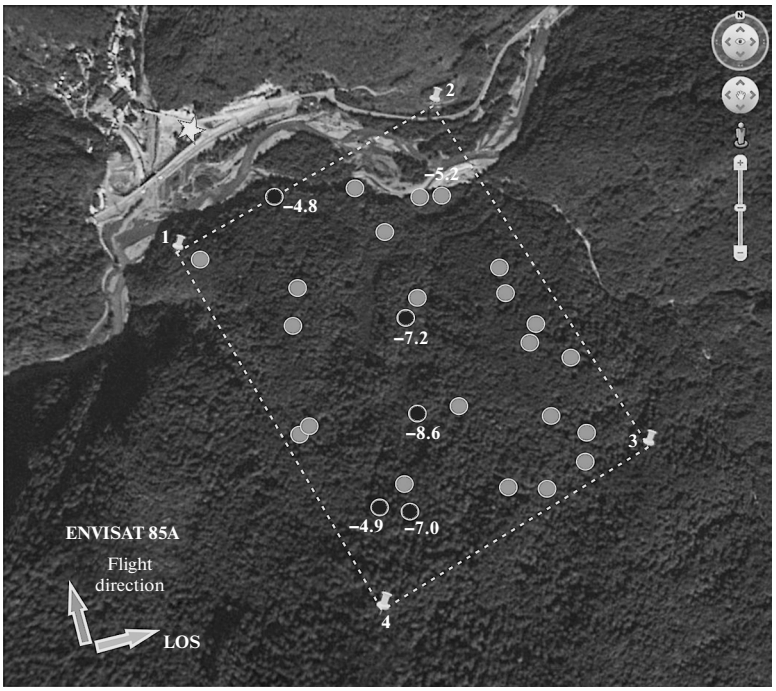

Fig. 3. The PSs identified on the landslide slope near Kepsha village from the ENVISAT data (ascending track 85A, survey period May 2006 to February 2009). The area of interest is shown by the box. The PSs with the low LOS displacement velocities ($|V_{LOS}| <$ 3 mm per annum) are shown gray. The PSs whose *LOS* projection of the velocity vector is below zero are shown black. Since the negative displacements are assumed to correspond to the motion away from the satellite, then, with the northeastern exposure of the slope and with surveying from the ascending track, $V_{LOS} < 0$ corresponds to the downward motion on the slope. The figures show the average *LOS* velocities in mm per annum. The reference area is shown by the asterisk.

the landslide slope near Kepsha village. The calculations are based on a series of ENVISAT and ALOS images. The reference area, marked by an asterisk in the figures, was selected by the procedure described above. In all cases, the variance is at most 3 mm per annum and only for the results based on ALOS data it attain 5 mm per annum.

The number of the persistent scatterers identified on this slope turned out to be sufficient for estimating the displacements. The position of the PSs on the landslide near Kepsha village determined from the data of different satellites is satellite-specific, because the images used for these calculations were acquired in different frequency bands from both the ascending and descending tracks, and they cover different time intervals.

In 2009, the lower part of the Kepsha landslide slope was deforested and the power electric line was constructed. Besides, at the foot of the slope (in the northwestern part of the studied area), the construction camp was built (Fig. 6). Due to this, the number of PSs identified from the images corresponding to ENVISAT track 35D (from November 29, 2010 to March 23, 2012) in the lower part of the slope has significantly increased. We have also processed the images from the TerraSAR X-band satellite (track 107D, acquisition period from July 13, 2012 to January 16, 2013). This analysis identified the PSs almost exclusively in the lower part of the landslide, where artificial objects appeared as a result of building. Therefore, these results are poorly suited for monitoring the forested part of the landslide and are therefore not considered here.

For the landslide near Kepsha village, the LOS displacement velocities (V_{LOS}) according to the ENVISAT data do not exceed 10 mm per annum. The estimates based on the ALOS data are somewhat higher; however, here, it should be taken into account that the positions of the identified PSs do not coincide. The rms deviation of the LOS velocities is at most 3–5 mm per annum. Thus, this landslide has been moderately stable since at least 2004. We note however that deforesting in the lower part of the landslide mass and exploitation of the railroad tunnel that is dug through this massif can trigger the activation of landslide processes. Therefore, it would be reasonable to continue monitoring the activity of the slope in this area.

We note that comparing the data from the ascending and descending tracks is a difficult task, since they correspond to the projection of the velocity vector on significantly different directions (shown in Figs. 3–6). The exposure of the landslaide slope near Kepsha village is such that the LOS displacements are negative for the ascending orbital tracks and positive for the descending tracks (see Figs. 3–6). If the data on the displacements are available from two tracks for approximately the same period, it is possible to determine the direction of the displacement vector assuming that the displacements occur along the topo-

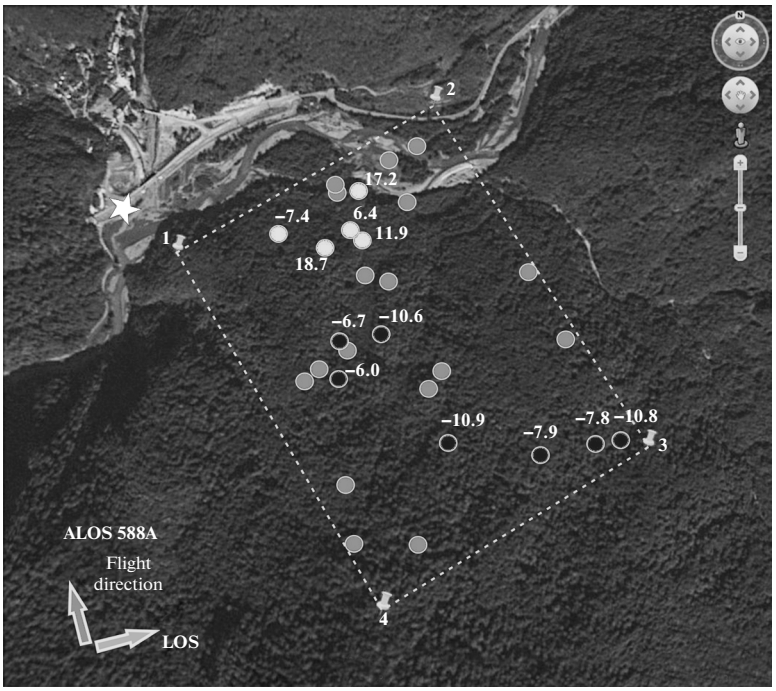

Fig. 4. The same as Fig. 3, ALOS data acquired from the ascending 588A track from January 2007 to September 2010. The white areas correspond to the PSs moving towards the satellite. The area within the white PS is deforested, and there are new engineering objects installed. The Google Earth optical images used in the study are taken before the beginning of the building operations.

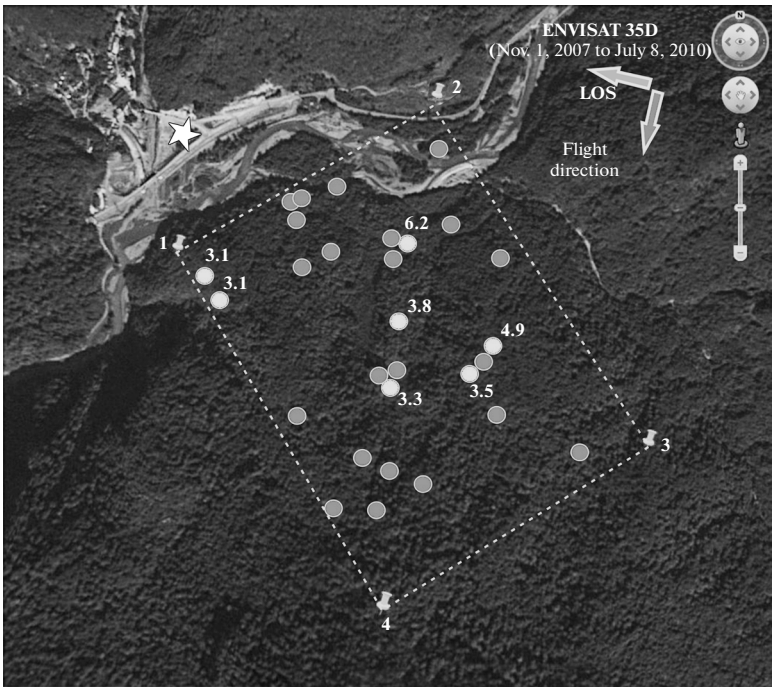

Fig. 5. The same as Figs. 3 and 4, ENVISAT data acquired from the descending 35D track during the interval of November 2007 to July 2010. For the descending track, the northeastward displacements are positive, i.e. directed opposite to *LOS*.

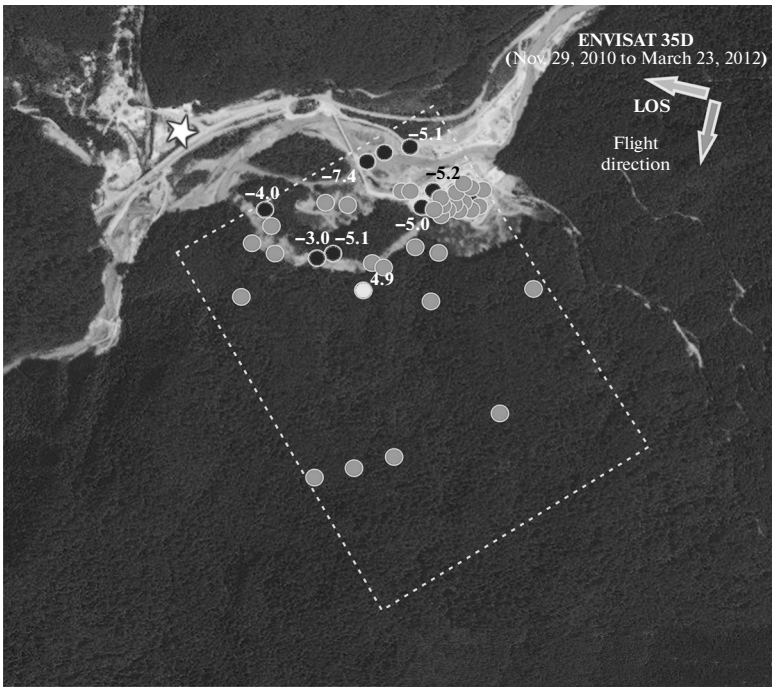

Fig. 6. The same as in Figs. 3–5, ENVISAT data acquired from the descending 35D track after orbit correction from November 29, 2010 to March 23, 2012. Just as in Fig. 5, the downward displacements along the slope are positive (directed opposite *LOS*).

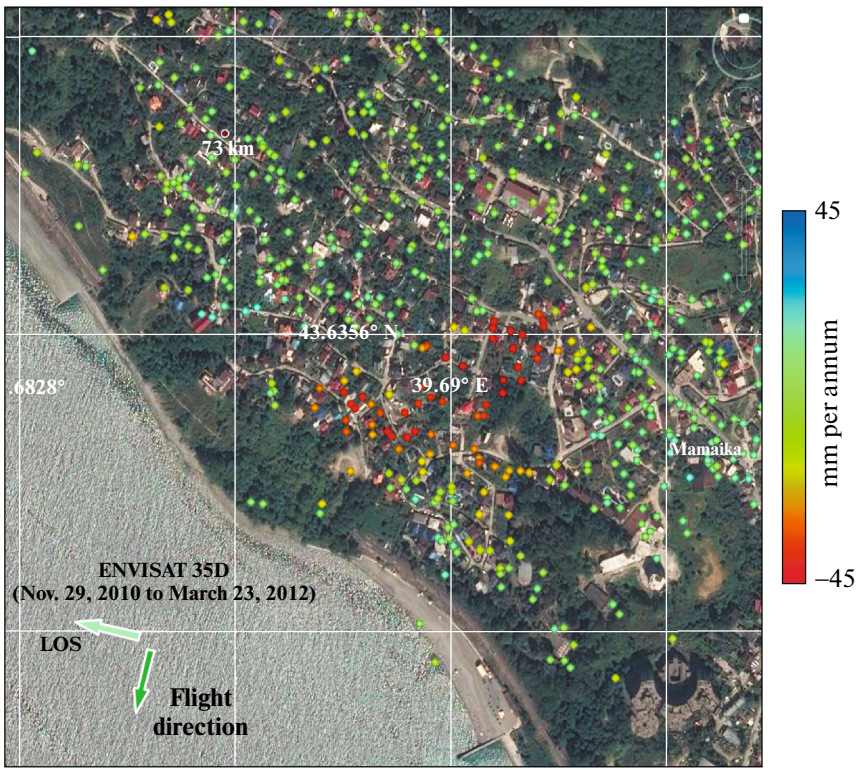

Fig. 7. The distribution of the OSs and their average displacement velocities on the landslide in Mamaika village obtained with the use of the StaMPS program package. The calculations are carried out from 13 images taken from descending track 35 of ENVISAT satellite from November 2010 to March 2012. The color scale shows the average *LOS* displacement velocities over the interval of the acquisition. The displacements directed away from the satellite (in this case, downwards along the slope) are shown red. The displacements that are close to zero are shown green.

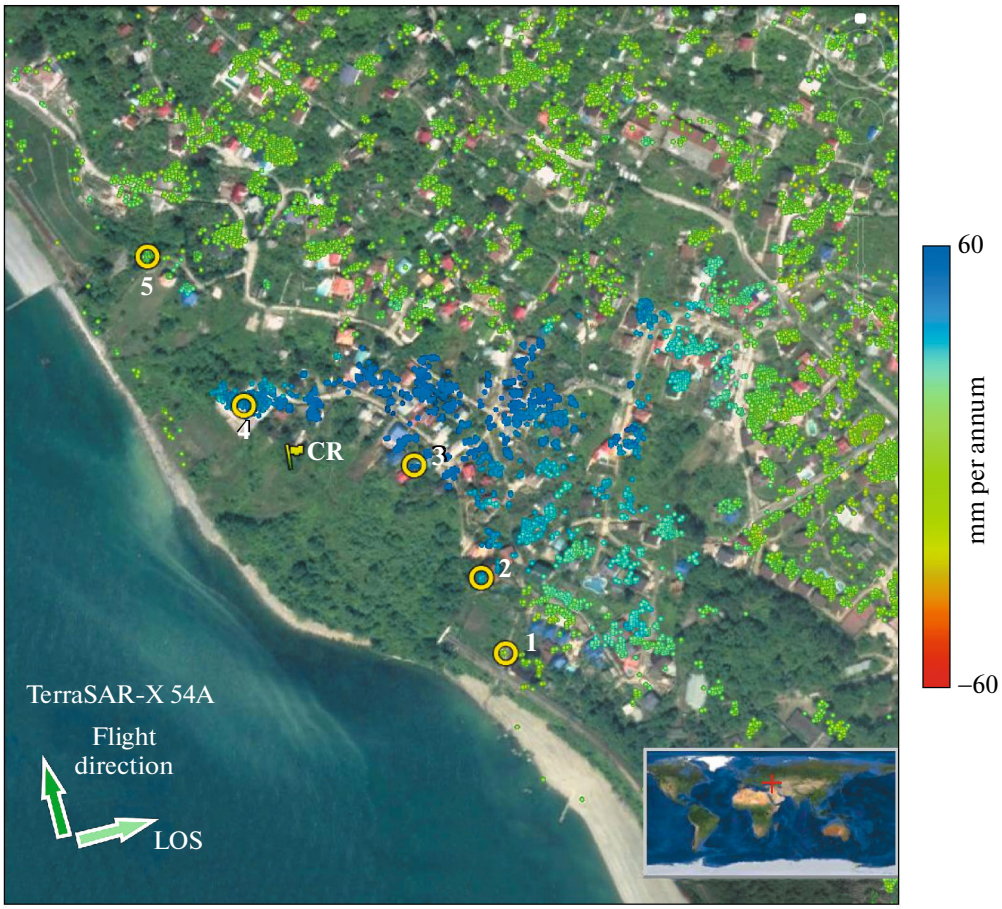

Fig. 8. The distribution of PSs and their average displacement velocities on the landslide in Mamaika village, which are obtained by the SB technology implemented in the StaMPS package. The calculations are conducted from 38 images acquired from TerraSAR satellite from December 24, 2011 to May 24, 2013. The color scale shows the average velocities in the direction of the satellite during the interval of acquisition. The displacements towards the satellite (in this case, downward the slope) are shown blue. The green areas correspond to the displacements that are close to zero. The time series of the displacements for the points marked by the yellow asterisks with figures are shown in Fig. 9. The location of the corner reflector is marked by the CR flag. The calculations are conducted from short-wavelewnght high-resolution images from the TerraSAR satellite in the region with a large number of building yield robust results, which do not depend on the processing method and the selection of the reference area.

graphic surface. The application of this approach to the Kepsha landslide in (Dmitriev et al., 2012) showed that the displacement vector is directed opposite to the gradient of the topography. Reconstruction of the displacement vector from its LOS projection in the context of this assumption demonstrated good agreement between the displacement velocities determined from different satellites and different tracks.

The results of calculating the average LOS displacement velocities (V_{LOS}) for the persistent scatterers identified on the landslide slope in Mamaika village from a series of ENVISAT images (descending track 35D (November 2010 to March 2012)) are illustrated in Fig. 7. The results for the Mamaika landslide from other series of ENVISAT images refer to the earlier time interval (before the intense building activities associated with the Olympiad in Sochi); therefore, we do not present them here.

Quite expectedly, from all the series of images, within the Mamaika landslide, significantly more persistent scatterers were identified than on the natural hillsides near Kepsha village. The particularly detailed results were inferred from the TerraSAR images. The images were taken by both satellites of the TerraSAR-X–TanDEM-X tandem pair. The images obtained from both satellites can be processed jointly; however, the spatial baselines between the TerraSAR-X and TabDEM-X satellites attain 200–300 m, which impedes the calculations. The attempts to obtain reliable results for the entire series of 38 images using the StaMPS PS method have been unsuccessful; however, the small-baseline (SB) technique implemented in the StaMPS package yielded good results. Using 152 interferometric pairs on the cropped part of the images, we identified 117306 PSs.

The results of processing the entire series of 38 TerraSAR images by the SB StaMPS method are shown in Fig. 8. The time coverage and the sizes of the baselines

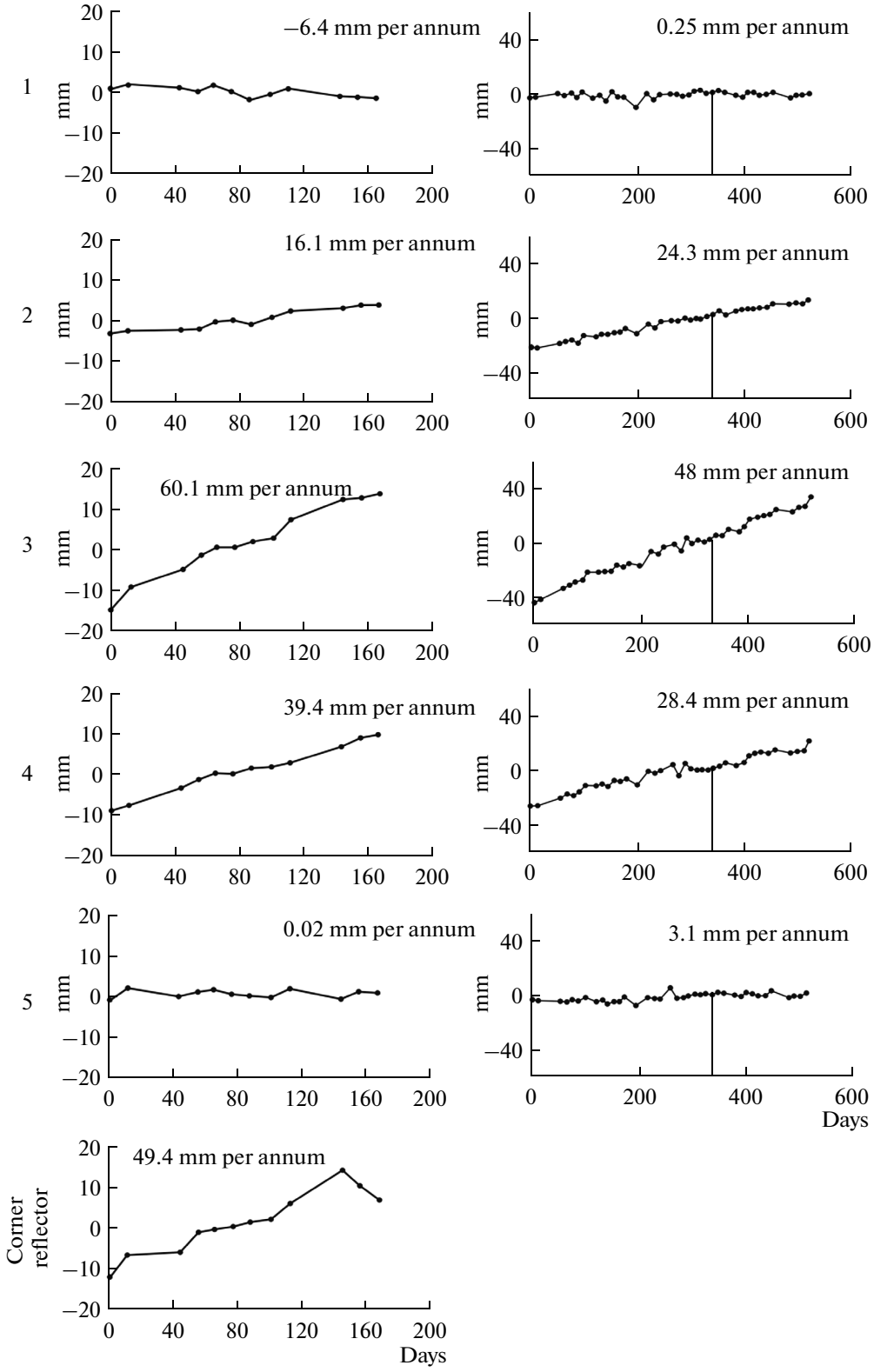

Fig. 9. The time series of *LOS* displacements for the points shown by the yellow circles with figures in Fig. 8 and for the corner reflector (CR). The left column of the graphs shows the displacements obtained by the processing of a series of 14 images acquired from the ascending track 54 of TerraSAR satellite from November 29, 2012 to May 24, 2013 (after the installation of the corner reflector on November 22, 2012). The processing is based on PS technology implemented in the StaMPS package. The right column of the graphs is the same obtained by the processing of 38 images (from December 24, 2011 to May 24, 2013) by the StaMPS small baseline method.

are presented in Fig. 1b. These results fully agree with those provided by the PS StaMPS method for the series of 14 images after the installation of the corner reflectors (shown by the gray circles in Fig. 1b). The coincidence of these results is illustrated by the time series shown in Fig. 9.

The Mamaika landslide is much more active than the landslide near Kepsha village. By processing the images from the ENVISAT and TerraSAR satellites, we managed to localize the area within the Mamaika landslide, where the LOS displacement velocities V_{LOS} attain 60 mm per annum (Figs. 7 and 8). We again note that, when comparing the results obtained from the ascending and descending tracks, one should take into account the exposure of the landslide slopes. This question is considered in more detail in (Mikhailov et al., 2013).

As shown by the calculations by different technologies, the estimates of the displacement field on this landslide are robust and they insignificantly depend on the processing strategy. The size of the landslide slope is 300 × 300 m. This area is confidently identified in the images from both satellites, i.e., from the ascending and descending tracks. The ground observations demonstrate significant surface deformations on this segment.

CONCLUSIONS

Although the environmental conditions in the Northern Caucasus are unfavorable for applying SAR interferometry, the obtained result show that the methods of persistent scatterers are efficient for monitoring the landslide processes even on the forested landslides. Considering the fact that landslide processes are quite widespread in the Northern Caucasus, SAR interferometry can be acknowledged as an efficient tool for monitoring the changes in the mobility of the landslide slopes.

Monitoring the landslide displacements on the mountain slopes of the Northern Caucasus can rely on radar images from satellites transmitting in the *L*-, *C*-, and *X*-bands. In order to increase the reliability of the obtained estimates of the displacements, it is preferable to use the images from both the low- and short-frequency bands.

Application of SAR interferometry in mountainous regions in conditions of densely vegetated terrains imposes special requirements on the strategy of processing and selecting the parameters of calculations. Particular attention should be paid to the selection of the cropped segment of the image and the reference area. The procedure for selecting the reference area based on analyzing the coherence maps, which is suggested in this paper, proved to be quite efficient. By applying this procedure, we obtained the consistent estimates of the average displacement velocities of landsliding near Kepsha village using the data from different satellites and different tracks. For the Mamaika landslide, within which there are a considerable number of good reflectors whose topography is quite smooth and low, the selection of the reference area is not vital. The best results for the Mamaika landslide are obtained with the use of the images from the short-wavelength TerraSAR satellite, while for the complex landslide conditions, such as the landslide near Kepsha village, the data from the longer-wavelength satellites are preferable.

Installation of an artificial corner reflector allowed us to estimate the displacement velocities of the landslide in the area where the natural persistent scatterers are absent from the TerraSAR data. A more reliable interpretation of the results of satellite SAR interferometry requires ground observations, which unfortunately were absent.

ACKNOWLEDGMENTS

We thank the European Space Agency (ESA) for providing the images from the ENVISAT satellite in the research project C1-7991. The ALOS images were purchased from Japan's Space Agency JAXA. The German Space Agency, DLR, has provided the TerraSAR images in research project LAN1247. We are grateful to A. Hooper (Leeds University, UK), as well as R. Hanssen, and S. Samiei-Esfahany (Delft Technological University, the Netherlands) for their valuable comments and advice on our study.

The work was supported by the Russian Science Foundation (grant no. 14-17-00094).

REFERENCES

Adam, N., Parizzi, A., Eineder, M., and Crosetto, M., Practical persistent scatterer processing validation in the course of the Terrafirma project, *J. Appl. Geophys.*, 2009, vol. 69, no. 1, pp. 59–65.

Brugioni, M., Mazzanti, B., Montini, G., and Sulli, L., Use of SAR interferometry for landslide analysis in the Arno river basin, *Proc. of the Second World Landslide Forum, October 3–7, 2011, Rome, Italy.*

Colesanti, C., Ferretti, A., Prati, C., and Rocca, F., Monitoring landslides and tectonic motion with the Permanent Scatterers technique, *Eng. Geol.*, 2003, vol. 68, pp. 1–14.

Colesanti, C. and Wasowski, J., Investigating landslides with space-borne Synthetic Aperture Radar (SAR) interferometry, *Eng. Geol.*, 2006, vol. 88, pp. 173–199.

Crosetto, M., Castillo, M., and Arbiol, R., Urban subsidence monitoring using radar interferometry: Algorithms and validation, *Photogram. Eng. Remote Sens.*, 2003, vol. 7, pp. 775–783.

Dmitriev, P.N., Golubev, V.I, Isaev, Yu.S., Kiseleva, E.A., Mikhailov, V.O., and Smol'yaninova, E.I., Some problems of processing and interpretation of the data of satellite radar interferometry by the example of monitoring the landslide processes, *Sovremennye Problemy Distantsionnogo Zondirovaniya Zemli iz Kosmosa*, 2012, vol. 9, no. 2, pp. 130–142.

Farina, P., Colombo, D., Fumagalli, A., Marks, F., and Moretti, S., Permanent scatterers for landslide investiga-

tions: outcomes from the ESA-SLAM project, *Eng. Geol.*, 2006, vol. 88, pp. 200–217.

Farina, P., Casagli, N., and Ferretti, A., Radar-interpretation of InSAR measurements for landslide investigations in civil protection practices, *Proc. First North American Landslide Conference, June 3–8, 2007, Vail, Colorado*, 2007, pp. 272–283.

Ferretti, A., Prati, C., and Rocca, F., Nonlinear subsidence rate estimation using permanent scatterers in differential SAR interferometry, *IEEE Trans. Geosci. Remote Sens.*, 2000, vol. 38, no. 5, pp. 2202–2212.

Ferretti, A., Prati, C., and Rocca, F., Permanent scatterers in SAR interferometry, *IEEE Trans. Geosci. Remote Sens.*, 2001, vol. 39, no. 1, pp. 8–20.

Ferretti, A., Fumagalli, A., Novali, F., Prati, C., Rocca, F., and Rucci, A., A new algorithm for processing interferometric data-stacks: SqueeSAR, *IEEE Trans. Geosci. Remote Sens.*, 2011, vol. 49, no. 9, pp. 3460–3470.

Hooper, A., Zebker, H., Segall, P., and Kampes, B., A new method for measuring deformation on volcanoes and other natural terrains using InSAR persistent scatterers, *Geophys. Res. Lett.*, 2004, vol. 31, L23611. doi: 10.1029/2004GL021737

Hooper, A., Segall, P., and Zebker, H., Persistent scatterer InSAR for crustal deformation analysis, with application to Volcán Alcedo, Galápagos, *J. Geophys. Res.*, 2007, vol. 112, B07407. doi: 10.1029/2006JB004763

Hooper, A., Spaans, K., Bekaert, D., Cuenca, M.C., Arikan, M., and Oyen, A., *StaMPS/MTI Manual*, Delft: Delft Institute of Earth Observation and Space Systems, Delft University of Technology, 2010. http://radar.tudelft.nl/~ahooper/stamps/StaMPS_Manual_v3.2.pdf.

Kimura, H. and Yamaguchi, Y., Detection of landslide areas using satellite radar interferometry, *Photogramm. Eng. Remote Sens.*, 2000, vol. 66, no. 3, pp. 337–344.

Lyons, S. and Sandwell, D., Fault creep along the southern San Andreas from interferometric synthetic aperture radar, permanent scatterers, and stacking, *J. Geophys. Res.*, 2003, vol. 108, no. B1, 2047. doi: 10.1029/2002JB001831

Meisina, C., Zucca, F., Conconi, F., Verri, F., Fossati, D., Ceriani, M., and Allievi. J., Use of Permanent Scatterers technique for large-scale mass movement investigation, *Quat. Int.,* 2007, vols. 171–172, pp. 90–107.

Mikhailov, V.O., Nazaryan, A.N., Smirnov, V.B., Diament, M., Shapiro, N., Kiseleva, E.A., Tikhotskii, S.A., Polyakov, S.A., Smol'yaninova, E.I., and Timoshkina, E.P., Joint inversion of the differential satellite nterferometry and GPS data: A case study of Altai (Chuia) earthquake of September 27, 2003, *Izv., Phys. Solid Earth*, 2010, vol. 46, no 2, pp. 91–103.

Mikhailov, V.O., Kiseleva, E.A., Dmitriev, P.N, Golubev, V.I, Smolyaninova, E.I., and Timoshkina, E.P., Estimation of full vector of displacements of the Earth' surface and technogenic objects based on InSAR data applied to oil and gas production areas, *Geofiz. Issled.,* 2012, vol. 13, no. 3, pp. 5–17.

Mikhailov, V.O., Kiseleva, E.A., Smolyaninova, E.I., Dmitriev, P.N., Golubeva, Yu.A., Isaev, Yu.S., Dorokhin, K.A., Timoshkina, E.P., Khairetdinov, S.A., and Golubev, V.I., Landslide monitoring at the North Caucasus rail road using SAR data of different wavelength and corner reflector, *Geofiz. Issled.,* 2013, vol. 14, no. 4, pp. 5–22.

Translated by M. Nazarenko